IEEE Access
Multidisciplinary | Rapid Review | Open Access Journal

Received September 22, 2019, accepted October 18, 2019, date of publication October 22, 2019, date of current version October 31, 2019.

Digital Object Identifier 10.1109/ACCESS.2019.2948837

Integrated Velocity Measurement Algorithm Based on Optical Flow and Scale-Invariant Feature Transform

XIAOCHEN LIU[1], XIAOTING GUO[1], DONGHUA ZHAO[1], HUILIANG CAO[1], JUN TANG[1], CHENGUANG WANG[2], CHONG SHEN[1], (Member, IEEE), AND JUN LIU[1], (Senior Member, IEEE)

[1]Key Laboratory of Instrumentation Science & Dynamic Measurement, Ministry of Education, School of Instrument and Electronics, North University of China, Taiyuan 030051, China
[2]School of Information and Communication Engineering, North University of China, Taiyuan 030051, China

Corresponding authors: Chenguang Wang (wangchenguang@nuc.edu.cn), Chong Shen (shenchong@nuc.edu.cn), and Jun Liu (liuj@nuc.edu.cn)

This work was supported in part by the National Natural Science Foundation of China under Grant 61603353, Grant 51705477, and Grant 61973281, in part by the Pre-research Field Foundation under Grant 6140518010201, in part by the Scientific and Technology Innovation Programs of Higher Education Institutions in Shanxi under Grant 201802084, in part by the Aeronautical Science Foundation of China under Grant 2018ZCU0002, in part by the Weapons and Equipment Joint Foundation under Grant 6141B021305, in part by the Program for the Top Young Academic Leaders of Higher Learning Institutions of Shanxi, in part by the Young Academic Leaders Foundation in North University of China, in part by the Science Foundation of North University of China under Grant XJJ201822, in part by the Fund for Shanxi "1331 Project" Key Subjects Construction, and in part by the 15th Graduate Science and Technology Project of North University of China under Grant 20181537.

ABSTRACT The pyramid Lucas-Kanade (LK) optical flow algorithm has been widely used in velocity measurement applications. However, these applications are limited by some shortcomings of the algorithm, such as its slow calculation speed and susceptibility to illumination changes. To solve these problems, a data fusion scheme based on the scale-invariant feature transform (SIFT) and optical flow is proposed to alleviate the dependence of the optical flow on the illumination conditions. In addition, an improved cubature Kalman filter (CKF) based on multi-rate residual correction (CKF-MRC) is proposed to solve the problem of inconsistency between the sampling frequencies of the SIFT and the optical flow, and takes full advantage of the high sampling frequency of SIFT. The experimental results demonstrate that the proposed CKF-MRC method can effectively improve the accuracy of velocity measurement under variable illumination conditions with a high sampling frequency.

INDEX TERMS Cubature Kalman filter, optical flow, residual error correction, scale-invariant feature transform.

I. INTRODUCTION

In recent years, rapid progress has been made in the development of unmanned aerial vehicle (UAV) technology. UAVs have been widely used in fields such as reconnaissance, military strikes, aerial photography, mapping and emergency rescue [1]–[5]. In addition, the optical flow navigation method inspired by insect motion is playing an increasingly important role in navigation in GPS-signal-denied environments. Optical flow (OF) can be regarded as the 2D projection movement of the 3D motion of observed objects [6]–[10]. The bioinspired OF navigation scheme has been developed accordingly, with superior properties that include small device volume, low power requirements, high autonomy and low cost, which are especially important in UAV navigation applications [11]–[13].

When OF is used as the sole navigation scheme, it can easily be disturbed by the surrounding environment, which leads to reduced navigation accuracy. Many researchers have made corresponding improvements to make the OF algorithm conform to a variety of environments. For example, [14] proposed an information fusion method based on a micro-electromechanical systems-based inertial measurement unit (MEMS-IMU) and OF, which was used to correct the MEMS-IMU's attitude when it diverged; simulation results showed that modification of the vehicle attitude in combination

The associate editor coordinating the review of this manuscript and approving it for publication was Yang Li.

with OF provided good performance, with the advantages of smaller errors, slow divergence and improved robustness. In [15], a vision-based UAV navigation method for use in urban and canyon environments was proposed; UAV navigation experiments in linear, L-shaped and T-shaped canyons were completed using OF as calculated from image sequences taken by the airborne camera. In [16], OF is used as a velocity measurement method to estimate the forward velocity of a quadrotor UAV. A control strategy for UAV hovering and forward motion in different flight modes based on a visual navigation system was proposed and UAV navigation based on OF was realized. In the above research, OF was used as a navigation assistant or a velocity measurement method to complete the navigation tasks. However, when the UAV performs fast movements, the traditional OF algorithm is no longer applicable and it is necessary to use the image pyramid method, which inevitably reduces the real-time performance of the OF algorithm. Additionally, while the OF algorithm offers high velocity measurement accuracy, it is vulnerable to changes in the illumination, which is one of the most important problems with the algorithm and must be solved.

As a feature matching algorithm, the scale-invariant feature transform (SIFT) maintains invariance to rotation, scaling and illumination variations and thus has wide application prospects in UAV navigation. Reference [17] used a SIFT algorithm to recognize landmarks and an extended Kalman filter to update the position; use of the A-star algorithm for path planning and the virtual force method for autonomous navigation of a mobile robot was then proposed, and finally, the effectiveness and applicability of the proposed method were demonstrated experimentally using the mobile robot. Reference [18] proposed a hybrid structure containing a convolutional neural network (CNN) and local image features to achieve first-person vision (FPV) pedestrian navigation, where a SIFT-based tracking algorithm was used to estimate motion and track each frame of the FPV image. To obtain higher homing precision for local robot navigation, a novel robot visual homing algorithm was proposed that combined SIFT features with the warping method [19], and the effectiveness of the proposed algorithm was verified experimentally. Reference [20] proposed a matching method based on SIFT feature saliency analysis to achieve robust feature matching between images that contained repetitive structures; feature matching was only to be performed within the region of interest to reduce the ambiguity caused by the repetitive structures, and the experimental results demonstrated the efficiency and robustness of the proposed method. While SIFT has wide application prospects in navigation, its low accuracy and poor robustness have limited further development.

Motivated by the analysis above, this paper investigates an OF/SIFT-based integrated velocity measurement system based on a multi-rate residual correction data fusion algorithm. In our study, OF and SIFT fusion is used as an improved scheme for UAV velocity measurements to solve the poor accuracy problem of OF under variable illumination conditions. In the data fusion process, because the OF calculation is dependent on the pyramid Lucas-Kanade (LK) algorithm, which has poor real-time performance while SIFT has high real-time performance, lack of synchronization between the two data sets will affect fusion accuracy. An improved cubature Kalman filter (CKF) algorithm based on residual correction is thus proposed to realize seamless fusion of the two data sets at different sampling frequencies. The main contributions of this paper are described as follows:

- To address the problem of the large errors in OF velocity calculations under the condition where there is varying illumination or shade, an OF/SIFT integrated velocity measurement system is proposed. Using the invariance of SIFT to change the brightness, the OF fault tolerance to changes in illumination is improved.
- To address the fusion problem caused by the different sampling frequencies used for OF and SIFT, a multi-rate fusion algorithm based on residual correction is proposed. In the overlap time period of the OF and the SIFT data, a CKF based on residual correction is implemented. At the low-rate OF data interval, only the time update and the residual correction of SIFT data are performed. Finally, seamless fusion and output of the two data sets are realized.

The rest of this paper is organized as follows. The principle and derivation of the pyramid LK optical flow algorithm and the SIFT algorithm are introduced in Section 2. In Section 3, the model and the proposed strategy are given. The experimental equipment is introduced in Section 4 and experimental results are presented that verify the effectiveness of the proposed algorithm. The paper ends with a few concluding remarks in Section 5.

II. ALGORITHM INTRODUCTION

A. PYRAMID LK OPTICAL FLOW ALGORITHM

OF represents the instantaneous velocity of a moving object. The LK algorithm involves three assumptions [21]: (i) brightness constancy; (ii) time is continuous or the motion is a small movement; and (iii) the space is consistent. From hypothesis (i), we can deduce the optical flow restriction equation as follows:

$$I(x, y, t) = I(x + dx, y + dy, t + dt). \tag{1}$$

where $I(x, y, t)$ represents the brightness of the point (x, y) at time t; in accordance with hypothesis (ii), i.e., assuming that the pixel movement is small enough, the Taylor formula can be applied to (1) and the higher order term can be ignored to give:

$$\frac{\partial I}{\partial x}dx + \frac{\partial I}{\partial y}dy + \frac{\partial I}{\partial t}dt = 0. \tag{2}$$

Substitution of (2) into (1) gives:

$$I_x v_x + I_y v_y + I_t = 0. \tag{3}$$

where $v_x = \frac{dx}{dt}$ and $v_y = \frac{dy}{dt}$, which are the optical flow velocities in the horizontal and vertical directions, respectively, can

change (3) into the following matrix form.

$$\begin{bmatrix} I_{x_1} & I_{y_1} \\ I_{x_2} & I_{y_2} \\ \cdots & \cdots \\ I_{x_n} & I_{y_n} \end{bmatrix} \begin{bmatrix} v_x \\ v_y \end{bmatrix} = - \begin{bmatrix} I_{t_1} \\ I_{t_2} \\ \cdots \\ I_{t_n} \end{bmatrix} \tag{4}$$

A weight function w is then set to enhance the influence of the OF value that is closest to the center point and (4) is solved using the least squares method.

$$\begin{bmatrix} v_x \\ v_y \end{bmatrix} = \begin{bmatrix} \sum wI_x^2 & \sum wI_xI_y \\ \sum wI_xI_y & \sum wI_y^2 \end{bmatrix}^{-1} \begin{bmatrix} -wI_xI_t \\ -wI_yI_t \end{bmatrix} \tag{5}$$

The LK algorithm is still deficient in its ability to solve for rapid motion of the vehicle [22]–[25]; therefore, to solve this problem, the concept of the Gaussian image pyramid, which satisfies the small motion hypothesis by constantly dividing the image OF in half, is introduced to solve the high-precision OF information. First, the image is semi-segmented from the bottom up to the top layer of the image pyramid and the OF is then calculated at the top of the image pyramid; the motion estimation results are used as the initial values for the next layer and the above process is repeated to the bottom of the pyramid. In this way, the possibility of failing to satisfy the motion hypothesis can be minimized.

OF offers high accuracy as a velocity measurement method, but the OF algorithm is susceptible to the effects of changes in the illumination, which causes large errors. It is thus necessary to find a velocity measurement method that is not affected by such illumination changes.

B. VELOCITY CALCULATION METHOD BASED ON SIFT

As a feature-based image matching algorithm, SIFT can calculate the movement distance of pixels based on their matched feature points, and can then transform the coordinate system to obtain the velocity of a UAV relative to the ground. Furthermore, the SIFT algorithm is invariant to illumination changes and scale transformations, and can be integrated with the OF algorithm to reduce the effects of illumination changes on the OF algorithm. The first step in the SIFT algorithm is to establish the difference of Gaussian (DOG) [26]–[28] scale space for extremum detection; the scale space can be obtained by convolution of the Gaussian function and the image:

$$L(x, y, \sigma) = G(x, y, \sigma) * I(x, y). \tag{6}$$

where $G(x, y, \sigma)$ is the Gaussian smoothing kernel function:

$$G(x, y, \sigma) = \frac{1}{2\pi\sigma^2} e^{-(x^2+y^2)/2\sigma^2}. \tag{7}$$

The value of σ in (6) and (7) determines the smoothness of the image. As the value of σ increases, the resolution of the image decreases in tandem. To detect stable key points effectively in the scale space, a Gaussian difference scale space, i.e., an image pyramid, is used:

$$\begin{aligned} D(x, y, s) &= (G(x, y, ks) - G(x, y, s)) * I(x, y) \\ &= L(x, y, k\sigma) - L(x, y, \sigma). \end{aligned} \tag{8}$$

To find the extreme points within the scale space, each sampling point should be compared with 26 points that include 8 adjacent points of the same scale and 9×2 points corresponding to the upper and lower adjacent scales. If it is the maximum or minimum of these points, the sampling point will then be considered to be a key point of the image in the scale space. After scale space extremum detection, only the extremum points in discrete space can be obtained. Therefore, it is necessary to fit the three-dimensional quadratic function to locate the key points accurately to obtain exact location information. The extremum points detected in the discrete space of two-dimensional functions do not usually overlap with the true extremum points in the continuous space. In eliminating any unqualified key points, the Taylor quadratic expansion given in (9) is used to fit the curve. The principal curvature of the point is then calculated using the Hessian matrix given in (10) to remove the key points of the local curvature asymmetry in the Gaussian difference scale space.

$$D(x) = D + \frac{\delta D^T}{\delta x} x + \frac{1}{2} x^T \frac{\delta^2 D}{\delta x^2} x \tag{9}$$

$$H = \begin{bmatrix} D_{xx} & D_{xy} \\ D_{xy} & D_{yy} \end{bmatrix} \tag{10}$$

Next, the key points of an image can be completely determined and precisely positioned, and which have scale invariance. On the other hand, in order to make the key points rotate invariantly, a main direction should be assigned to each key point. A gradient histogram is used to calculate the gradient directions of neighboring pixels; then, based on the peak value of the histogram, the main direction can be determined, while the remaining 80% of the maximum can be used as an auxiliary direction.

Based on the needs of later calculation, a feature descriptor should be established for each key point to make the key point have good robustness to factors such as illumination and perspective change. This descriptor contains not only the key point itself, but also other pixels around the key point that contribute to it. Moreover, the descriptor needs to be clearly differentiated to ensure the efficiency of subsequent registration. Establishment of descriptors: I. Rotate the axes in the same direction as the key points to ensure that the feature points have rotation invariance. II. It is necessary to determine the neighborhood range of the calculated feature descriptor, and divide the neighborhood near the feature point into 4×4 pixel-regions, each pixel-region as a seed point, which has 8 directions, as shown in Fig. 3; the gradient information for the 8 directions is calculated within the region and is represented by a 128-dimension vector.

The last step of the SIFT algorithm is feature point matching. The similarity between two SIFT descriptors is usually expressed using the Euclidean distance. By comparing the threshold with the Euclidean distance, the matching result can be obtained. After the pixel distance between two matching points is calculated, the velocity of the UAV relative to the ground can be obtained through coordinate transformations.

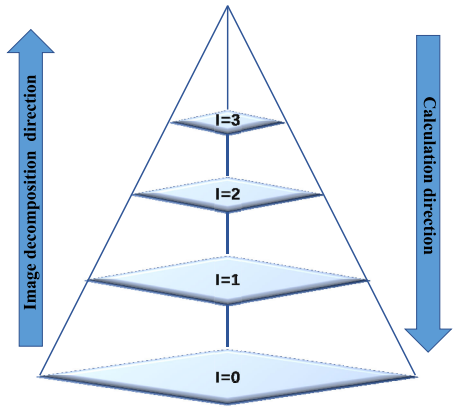

FIGURE 1. Image pyramid.

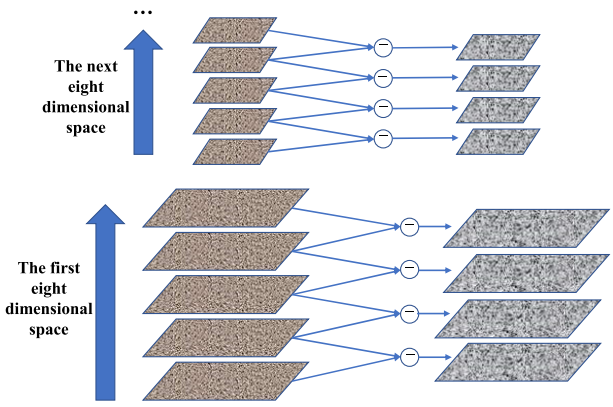

FIGURE 2. Gaussian difference scale space.

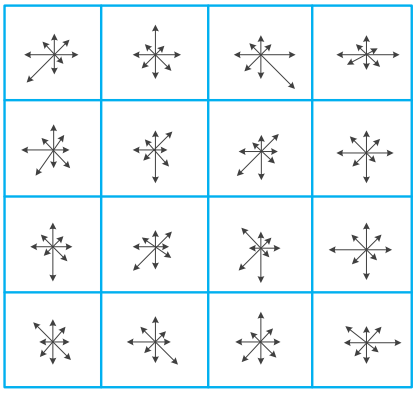

FIGURE 3. 4 × 4 pixel region showing the key points.

III. MODEL AND PROPOSED STRATEGY

A. DATA FUSION MODEL INTRODUCTION

The SIFT and OF data are fused to alleviate the effects of the illumination conditions on the flow accuracy, an algorithm called CKF-MRC (which is described in detail later in the paper) is used to seamlessly integrate SIFT and the OF data. The fusion model is shown in Fig. 4 and both the SIFT and the OF data have been converted into the ground velocity of the UAV.

Algorithm 1 Pyramid LK Algorithm

Input: Two frame pictures.
Algorithmic process:
  Build the image pyramid.
for $l_m = 0 : 1 : l_m$
  Layer 0 is the original picture.
  Scale the width and height of the image to half that of the original picture to the l_m layer.
end
for $l_m = l_m : 1 : 0$
  l_m layer optical flow is calculated as the initial value of the $l_m - 1$ layer.
  Until calculated to the $0th$ layer.
end
end

Algorithm 2 SIFT Algorithm

Input: Two frame pictures.
Algorithmic process:
- ➢ Extremum detection in the scale space.
- ➢ Key point generation.
  - Key point detection
  - Elimination of any unqualified key points
- ➢ Establishment of the key point feature information.
  - Determination of the main and auxiliary directions of the key points
  - Establishment of descriptors
- ➢ Key point matching.
- ➢ Obtaining the pixel moving distance.
- ➢ Obtaining the UAV velocity relative to the ground via coordinate system conversion.

B. MULTI-RATE DATA FUSION ALGORITHM BASED ON RESIDUAL CORRECTION

Because of the inconsistency between the data output rates of the OF algorithm and the SIFT algorithm, the problem of how to fuse data efficiently with the aim of guaranteeing accuracy has become a subject of considerable study. At present, the fusion algorithms used to address this problem are mainly based on the Kalman filter (KF). The cubature Kalman filter (CKF) algorithm is based on a Gaussian filter framework and has been used widely to perform precise fusion of navigation information. The CKF offers certain advantages in processing of nonlinear data; the specific steps of the CKF algorithm are described in detail in [29] and will thus not be repeated here, but the CKF is used as the main data fusion method this paper. The simplest data fusion strategy involves construction of a single-rate filter, as shown in Fig. 5. When the OF data coincides with the SIFT data, the CKF is used to fuse the data from the two algorithms. The velocity of the UAV output frequency is consistent with the OF output frequency and no parameter updates or calculations are carried out at other times.

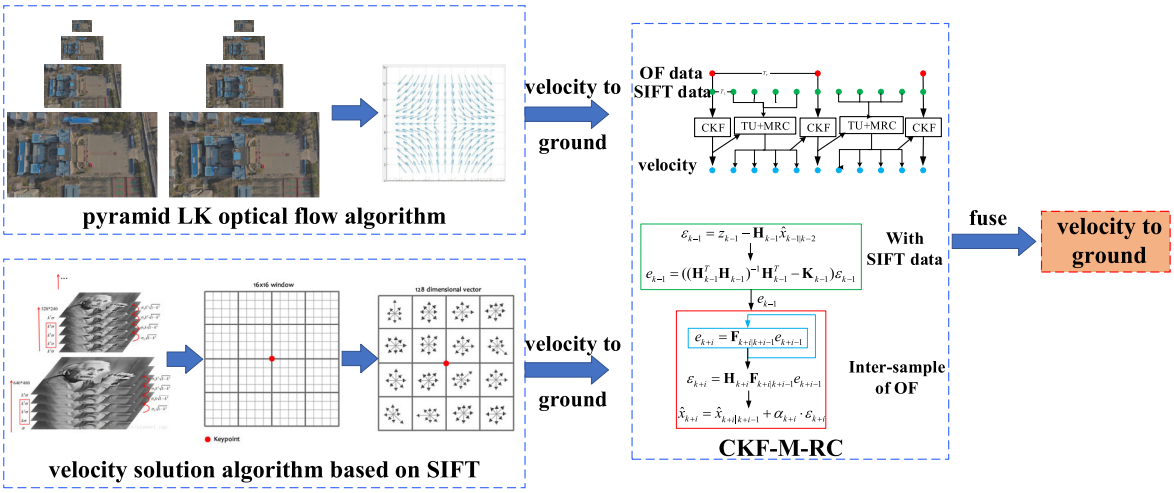

FIGURE 4. Data fusion model.

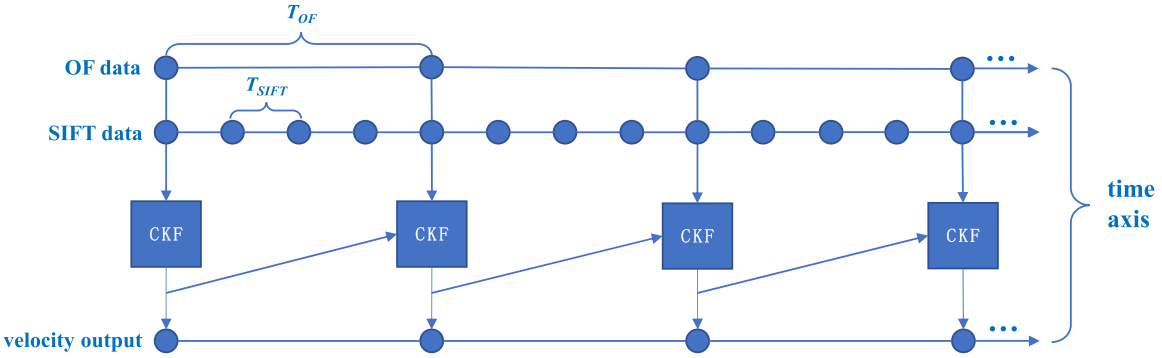

FIGURE 5. Single-rate filter structure.

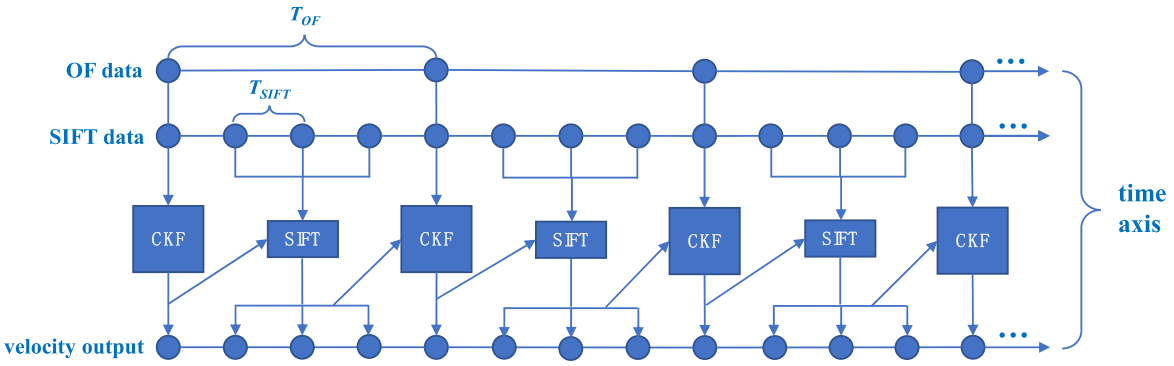

FIGURE 6. High-rate filter structure.

To make full use of the high-frequency SIFT data and ensure high-frequency output of the velocity, the method described above is modified. In the intervals of the low-frequency OF data, the high-frequency SIFT algorithm is used to calculate the velocity directly; the specific process is illustrated in Fig. 6.

While the output frequency of the velocity is increased to be the same as the output frequency of the SIFT, the filter parameters such as the filter gain, the covariance and the cross-covariance are not updated in time. The next step is to go further and use a multi-rate filter. The basic idea in this case is to divide the filtering process into two processes, i.e., the time update and the observation update, and perform these processes separately. When there are OF data, the complete filtering steps are performed; otherwise, only the time update process must be performed, as shown in Fig. 7.

In a conventional multi-rate filter algorithm, the velocity output frequency is the same as the output frequency of the high-frequency SIFT data, and the filter parameters can thus be updated in time. However, the estimation accuracy and

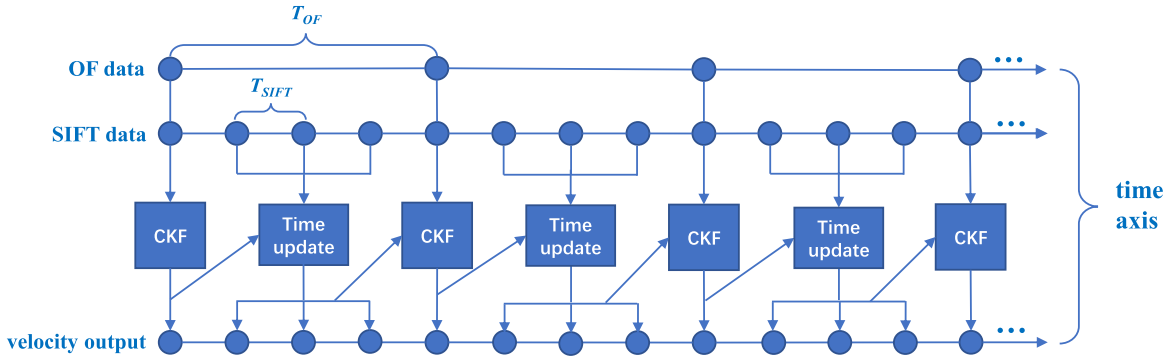

FIGURE 7. Multi-rate filter structure.

the convergence of the filter are uncertain when the OF data interval is not compensated with respect to the filter state. Therefore, an improved residual correction method for multi-rate data fusion estimation is proposed to correct the filter estimator at each instance of high-frequency data output.

The calculation methods for the state estimation errors and the residual errors are as follows:

$$e_t = x_t - \hat{x}_t \tag{11}$$

$$\sigma_t = y_t - H_t \hat{x}_{t|t-1}. \tag{12}$$

Here, (12) is derived as follows and (11) is obtained by substitution:

$$\begin{aligned}\sigma_t &= y_t - H_t \hat{x}_{t|t-1} \\ &= H_t x_t - H_t \hat{x}_{t|t-1} \\ &= H_t \Phi_{t-1} x_{t-1} - H_t \Phi_{t-1} \hat{x}_{t-1} \\ &= H_t \Phi_{t-1} e_{t-1}.\end{aligned} \tag{13}$$

Equation (13) can be recorded as $\sigma_t = f(e_{t-1})$, i.e., the residual can be represented by the state estimation error. Conversely, the state estimation errors can also be represented by the residual errors:

$$\begin{aligned}e_t &= x_t - \hat{x}_t \\ &= x_t - \hat{x}_{t|t-1} - k_t \left(y_t - H_t \hat{x}_{t|t-1}\right) \\ &= x_t - \hat{x}_{t|t-1} - k_t \sigma_t \\ &= \left(H_t^T H_t\right)^{-1} H_t^T \sigma_t - k_t \sigma_t \\ &= \left(\left(H_t^T H_t\right)^{-1} H_t^T - k_t\right) \sigma_t.\end{aligned} \tag{14}$$

where

$$\sigma_t \approx H_t \left(x_t - \hat{x}_{t|t-1}\right) \left(H_t^T H_t\right)^{-1}$$

$$H_t^T \sigma_t = \left(H_t^T H_t\right)^{-1} H_t^T H_t \left(x_t - \hat{x}_{t|t-1}\right)$$

$$x_t - \hat{x}_{t|t-1} = \left(H_t^T H_t\right)^{-1} H_t^T \sigma_t.$$

The observation noise is approximately zero and is thus omitted, while the matrix H is considered to be irreversible. Equation (14) can be recorded as: $e_t = g(\sigma_t)$, i.e., the residual can be expressed using the state estimation error. In addition, the self-propagation process of the state estimation error is considered to have the following form:

$$\begin{aligned}e_t &= x_t - \hat{x}_t \\ &= x_t - \hat{x}_{t|t-1} - k_t \left(y_t - H_t \hat{x}_{t|t-1}\right) \\ &= \left(x_t - \hat{x}_{t|t-1}\right) - k_t \left(H_t x_{t|t-1} + R_t - H_t \hat{x}_{t|t-1}\right) \\ &= \left(I - k_t H_t\right) \left(x_t - \hat{x}_{t|t-1}\right) - k_t R_t \\ &= \left(I - k_t H_t\right) \Phi_{t-1} e_{t-1} - k_t R_t.\end{aligned} \tag{15}$$

where, Φ_{t-1} is State transition matrix, and y_t is measurement variable. When the OF data coincide with the SIFT data, (12) and (14) can be used to calculate the state estimation error and the residual error. At the sampling interval of the OF data, where there are only SIFT data and no OF data, there is no way to obtain the residual error directly. However, according to (15), in the optical flow sampling interval where covariance matrix $R_t \to \infty$ and $k_t \to 0$. Therefore, only the filter parameters in the time update are meaningful and (15) can be modified to read:

$$e_t \approx \Phi_{t-1} e_{t-1}. \tag{16}$$

Because the results for R_t and k_t are unpredictable under the current circumstances, their product is omitted. In a conventional CKF, the optimization estimate of the state can be expressed as $\hat{x}_t = \hat{x}_{t|t-1} + k_t \sigma_t$. At the output interval of the OF data, the filter gain is theoretically very small, so the state estimation can be adjusted to read:

$$\hat{x}_t = \hat{x}_{t|t-1} + \kappa_t \cdot \hat{\sigma}_t. \tag{17}$$

where $\kappa_t = diag\left(\left[\kappa_{1,t}, \kappa_{2,t}, \cdots \kappa_{n,t}\right]\right)$, which acts as a parameter that is used to replace the filter gain in the conventional CKF, is used to determine both the bandwidth and the response speed of the filter. To get a higher precision fusion result, the proportional coefficient κ_t is selected by experience. $\hat{\sigma}_t$ is the estimated residual.

In general, in the presence of the OF data, a complete CKF based on residual correction ((12) and (14)) is used to filter and fuse the OF and SIFT data and then prepare for the updating cycle of the estimation error and the residuals in the next instant. In the absence of the OF data, (16) is then used

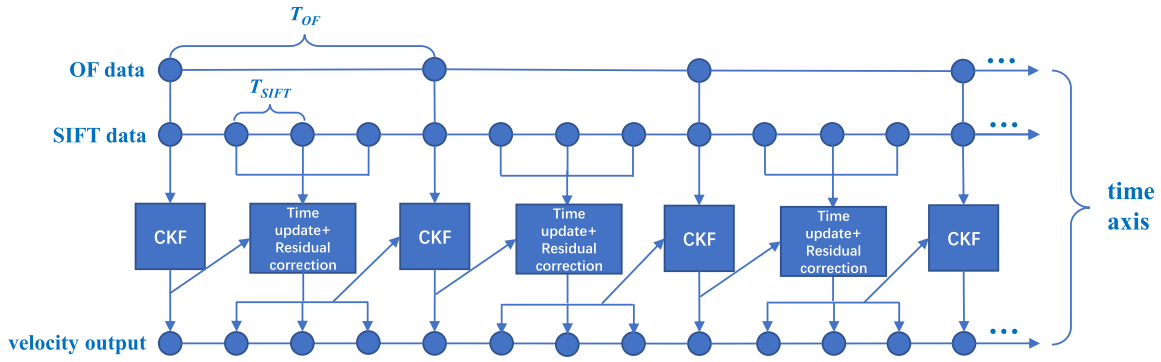

FIGURE 8. Multi-rate filter based on residual correction.

to update e_t, (13) is used to calculate the residual error, and finally (17) is used to calculate the state variables.

Algorithm 3 Multi-Rate Data Fusion Algorithm Based on Residual Correction

Algorithmic process:

➢ Judge whether there are optical flow data

■ Yes:

- (12) is used to calculate the state error.
- (14) is used to calculate the residual error.
- The CKF is used for data fusion.

■ No:

- (16) is used to update e_t.
- (13) is used to calculate the residual error.
- (17) is used to calculate the state variables.

IV. EXPERIMENT RESULTS AND DISCUSSION

In this section, to validate the efficiency and superiority of the proposed OF/SIFT fusion algorithm based on multi-rate residual correction (CKF-MRC) is tested via UAV experiments in two different places under different illumination conditions. The experimental locations are in the campus of the North University of China, Taiyuan. The NovAtel PW7720 Global Positioning System (GPS) receiver is used in this experiment as the high-precision velocity reference, and on the back of the GPS device antenna, there is an OF camera that is oriented vertically to the horizontal plane and is calibrated by the method in [30]. The OF camera and reference parameters are presented in Table 1. The experimental facilities are shown in Fig 9.

A. PERFORMANCE COMPARISON OF THE DIFFERENT ALGORITHMS

To demonstrate that the proposed algorithm can improve accuracy while ensuring the same output rate as that of SIFT, a series of experiments are carried out; for contrast, five additional fusion algorithms are added to the experiment (the classical EKF algorithm (EKF), the EKF fusion algorithm based on multi-rate filtering (EKF-M), the multi-rate EKF

TABLE 1. Camera and reference parameters.

Optical flow camera		GPS	
Sensor brand	IMX179		
Sensor category	CMOS		
Lens size	1/3.2inch	Brand	PW7720
Pixel size	1.4μm	Velocity accuracy	0.03m/s
Focal length	10mm	Position accuracy	1cm+1ppm
Max Sampling rate	120Hz	Time accuracy	20ns
Max resolution	1280*760		

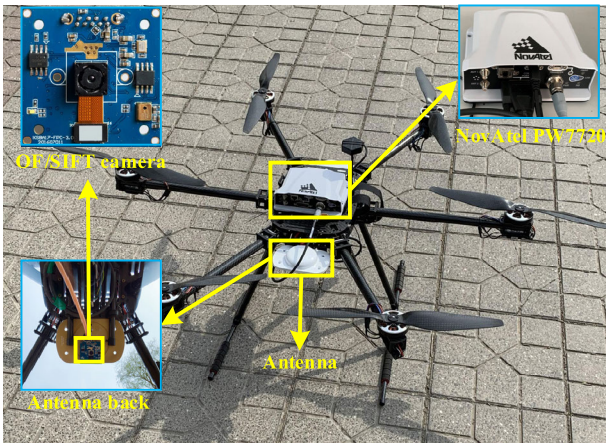

FIGURE 9. Experiment facilities.

fusion algorithm based on residual correction (EKF-M-RC), the classical CKF algorithm (CKF), and the CKF fusion algorithm based on multi-rate filtering (CKF-M)). In that, EKF and CKF are popularly used to data fusion. EKF and its derivative algorithms have simple algorithmic structure and advanced processing speed compare to CKF, on the opposite side, CKF and its derivative algorithms has higher nonlinear fitting accuracy. In order to explain the superiority in accuracy of the proposed algorithm, 4 experiments are carried out. In the experiments, the SIFT output rate is approximately 200/min, which is approximately five times that of the OF.

- *Experiment 1:* The UAV is in random motion at variable velocity at an altitude of 12 m. The flight time

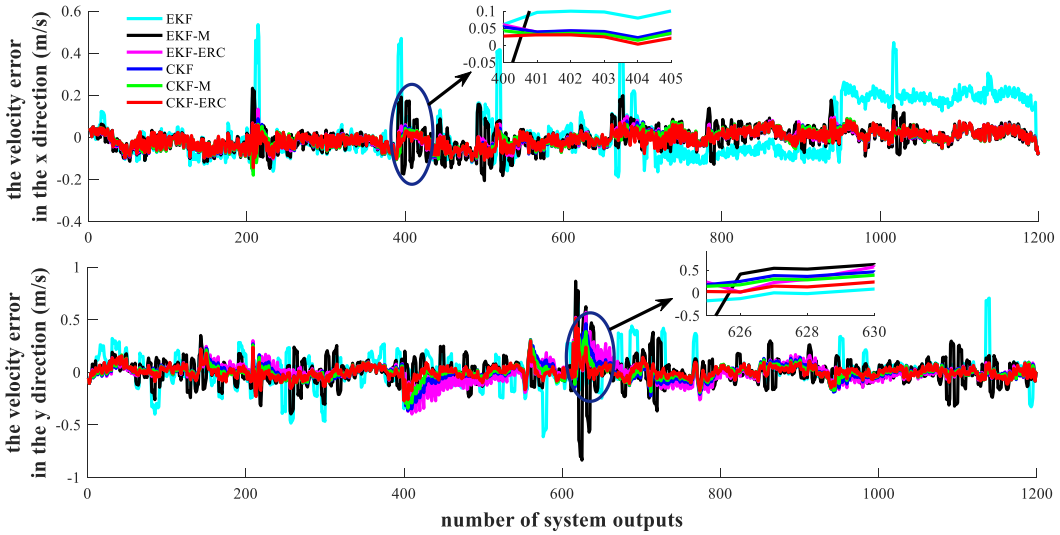

FIGURE 10. Velocity error characteristics of experiment 1.

is approximately 6 min and the camera's sampling frequency is 60 Hz.

- *Experiment 2:* The UAV is in random motion at variable velocity at an altitude of 30 m. The flight time is approximately 6 min and the camera's sampling frequency is 60 Hz.

After the number of moving pixels in the image coordinate system is calculated using OF and the SIFT algorithm, the ground velocity of the UAV can be obtained by fusing the three-dimensional attitude and height information provided by the reference source, and the data from OF and SIFT are assessed simultaneously according to the system time. The average reference velocity for experiment 1 is 10.35 m/s, while that of experiment 2 is 5.14 m/s. MATLAB is employed to get the velocity error curves for the six algorithms in the two experiments which are shown in Figs. 10 and 11, and the number of data of two groups processed are 1200, the processing time is 5.454589 s and 5.594431 s respectively.

Because the UAV uses a vehicle coordinate system with the default y axis as the forward direction, the motion component in the x direction is smaller and the fusion accuracy is higher. Figures 10 and 11 show that, because of the velocity nonlinearities caused by the irregular motion of the UAV, the EKF and related algorithms all have poor accuracy. When the velocity of the motion increases from 5 m/s to 10 m/s, the accuracy decreases for all the fusion algorithms, but the proposed CKF-MRC still provides a terrific performance. Furthermore, as mentioned above, the output speed of the OF is 40/min, and thus, in two sets of 6 min experiments, there are approximately 240 optical flow velocity outputs, although the final UAV velocity outputs are 1200. When compared with the purely OF system, the velocity output frequency of this system is higher. To demonstrate the superiority of the CKF-MRC algorithm more intuitively, the histograms shown in Figs. 12 and 13 are generated based on the variance and the root mean square error (RMSE) of the six algorithms. Because of the excellent performance of CKF-MRC, this algorithm will be used in the subsequent experiments.

B. PERFORMANCE COMPARISON OF THE DIFFERENT METHODS

Another purpose of data fusion between OF and SIFT is to alleviate the reduction in accuracy of the OF caused by light and shade changes. To illustrate the robustness of the fusion algorithm in velocity calculations when dealing with illumination changes, experiment 3 and experiment 4 are carried out:

- *Experiment 3:* The UAV is in random motion at variable velocity under varying light and shade conditions at an altitude of 12 m, and the camera's sampling frequency is 60 Hz, the running time is 1 min.
- *Experiment 4:* The UAV is in random motion at variable velocity under varying light and shade conditions at an altitude of 30 m, and the camera's sampling frequency is 60 Hz, the running time is 1 min.

In these experiments, the changes in the illumination are mainly caused by the occlusion by buildings and clouds because of the less distance in the sheltered area; additionally, the emphasis in this section is not placed on discussion of the differences in the data output frequency, but rather is on the accuracy of the velocity calculations under variable illumination conditions. To provide a better illustration of the problem, overlapping OF and SIFT data under light change conditions are acquired separately to perform the two experiments described above. In experiments 3 and 4, all of pictures that continuous change of light and shade are specially selected from normal experimental images. For example, we can select 60 pairs of images from 1200 pictures, all of which contain light and shade changes, each selected pair of pictures can obtain the corresponding reference data according to its original position and the experiment can be completed using 60 pairs of pictures. So, the experiments

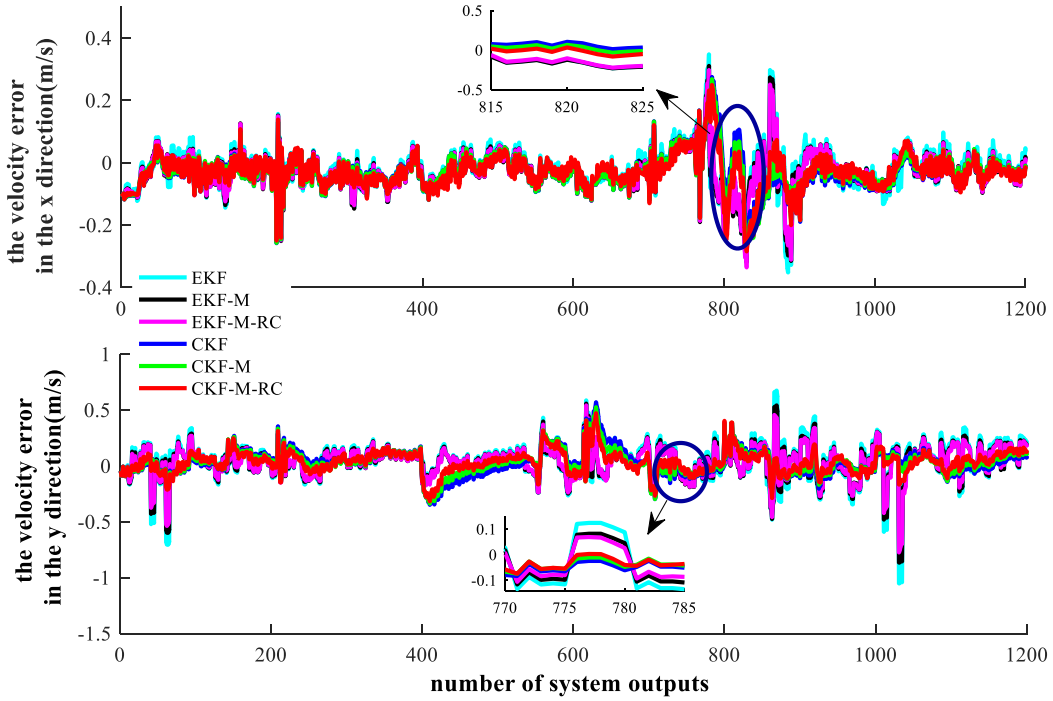

FIGURE 11. Velocity error characteristics of experiment 2.

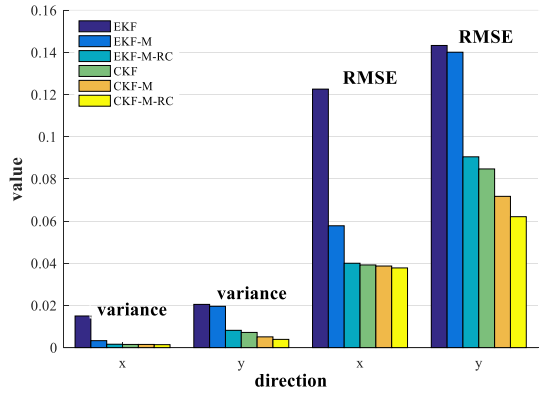

FIGURE 12. Variance and RMSE histogram for experiment 1.

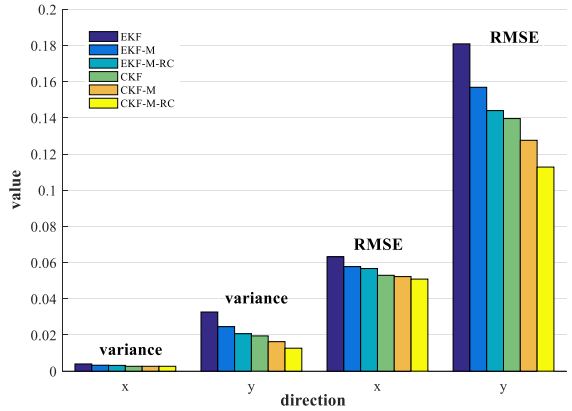

FIGURE 13. Variance and RMSE histogram for experiment 2.

assume that the output frequencies of the OF and the SIFT are equal, i.e., that all collected images with illumination changes

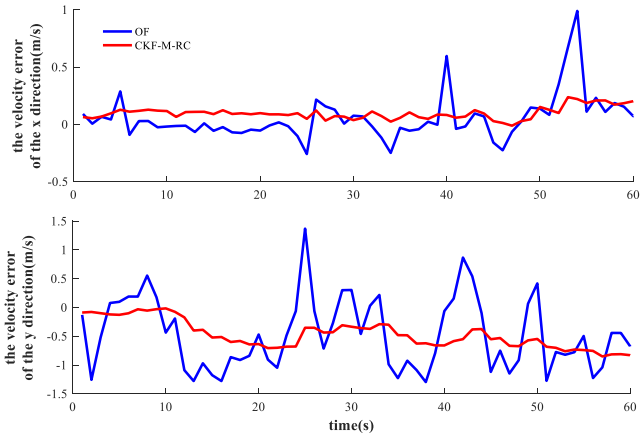

FIGURE 14. Comparison of velocity errors in experiment 3.

are processed by both SIFT and the OF algorithm, while the difference in output frequency between these algorithms is ignored; then, the calculated velocity is fused using the CKF-MRC algorithm and is compared with the velocity error of pure OF. The velocity error comparison curves are shown in Figs. 14 and 15.

The velocity error curves show that different illumination conditions have different effects on the OF accuracy. While the accuracy of the fusion algorithm is reduced because of the influence of the OF, it is still better than that of the pure OF. To describe the performance of the fusion algorithm in more detail, Table 2 and Table 3 list the quantified values of the variance and the RMSE for the two experiments. The numerical results verify that the performance of the fusion

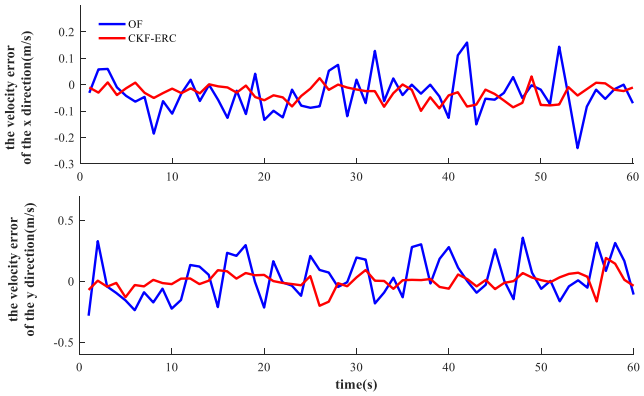

FIGURE 15. Comparison of velocity errors in experiment 4.

TABLE 2. Data variance and RMSE in experiment 3.

	Variance		RMSE	
	x	Y	x	y
OF	0.0672	0.5182	0.259	0.7199
CKF-M-RC	0.0057	0.0592	0.0763	0.2436

TABLE 3. Data variance and RMSE in experiment 4.

	Variance		RMSE	
	x	Y	x	y
OF	0.051	0.0292	0.071	0.1711
CKF-M-RC	0.0009	0.0039	0.0293	0.0638

algorithm is better than that of the pure OF algorithm under changing illumination conditions.

In fact, the influence of illumination with different heights of changing range on optical flow measurement is a research topic, which can be further studied in our future work. However, the comparison between the height of 12m and 30m in this experiment shows that: I. the proposed method is effective at different altitudes. II. The illumination variation has a greater impact on the accuracy of velocity measurement at lower flight altitudes.

V. CONCLUSION

This paper has proposed an OF and SIFT data fusion method called the CKF-MRC for UAV applications to enhance the velocity accuracy and the data output frequency of the OF algorithm in variable illumination environments. The CKF-MRC considers two main cases for data fusion. On the one hand, when the SIFT data coincide with the OF data, a complete CKF fusion process is performed to calculate the UAV velocity information. On the other hand, only a time update process is carried out and the estimated residual error is used to correct the filtering state when there are no OF data; therefore, higher fusion accuracy for the velocity can be obtained based on multi-rate filtering.

In future work, the authors intend to place greater emphasis on research into new advanced fusion algorithms. In addition, subsequent modification of the current fuse model for UAV velocity measurement to increase its intelligence will form another possible area for further investigation.

ACKNOWLEDGMENT

(Xiaochen Liu, Xiaoting Guo, and Huiliang Cao contributed equally to this work.)

We thank David MacDonald, MSc, from Liwen Bianji, Edanz Editing China (www.liwenbianji.cn/ac), for editing the English text of a draft of this manuscript.

AUTHOR CONTRIBUTIONS

Funding acquisition: Chong Shen, Jun Tang, Huiliang Cao and Xiaoting Guo. Investigation: Xiaochen Liu. Methodology: Xiaochen Liu, Chong Shen, Xiaoting Guo. Software: Huiliang Cao, Donghua Zhao, and Chenguang Wang. Writing–original draft: Xiaochen Liu. Writing–review & editing: Chong Shen, Jun Tang and Jun Liu.

REFERENCES

[1] M. Aljehani and M. Inoue, "Performance evaluation of multi-UAV system in post-disaster application: Validated by HITL simulator," *IEEE ACCESS*, vol. 7, pp. 64386–64400, 2019.

[2] N. Q. Truong, P. H. Nguyen, S. H. Nam, and K. R. Park, "Deep learning-based super-resolution reconstruction and marker detection for drone landing," *IEEE ACCESS*, vol. 7, pp. 61639–61655, 2019.

[3] C. Shen, Y. Zhang, J. Tang, H. Cao, and J. Liu, "Dual-optimization for a MEMS-INS/GPS system during GPS outages based on the cubature Kalman filter and neural networks," *Mech. Syst. Signal Process.*, vol. 133, no. 1, Nov. 2019, Art. no. 106222.

[4] H. Cao, Y. Zhang, C. Shen, Y. Liu and X. Wang, "Temperature energy influence compensation for MEMS vibration gyroscope based on RBF NN-GA-KF method," *Shock Vib.*, Dec. 2018, Art. no. 2830686. doi: 10.1155/2018/2830686.

[5] C. Shen, X. Liu, H. Cao, Y. Zhou, J. Liu, J. Tang, X. Guo, H. Huang, and X. Chen, "Brain-like navigation scheme based on MEMS-INS and place recognition," *Appl. Sci.*, vol. 9, no. 8, p. 1708, 2019.

[6] F. Martínez, A. Manzanera, and E. Romero, "Automatic analysis and characterization of the hummingbird wings motion using dense optical flow features," *Bioinspiration Biomimetics*, vol. 10, no. 1, 2015, Art. no. 016006.

[7] M. P. Rodriguez and A. Nygren, "Motion estimation in cardiac fluorescence imaging with scale-space landmarks and optical flow: A comparative study," *IEEE Trans. Biomed. Eng.*, vol. 62, no. 2, pp. 774–782, Feb. 2015.

[8] C. Shen, J. Yang, J. Tang, J. Liu, and H. Cao, "Note: Parallel processing algorithm of temperature and noise error for micro-electro-mechanical system gyroscope based on variational mode decomposition and augmented nonlinear differentiator," *Rev. Sci. Instrum.*, vol. 89, no. 7, 2018, Art. no. 076107.

[9] H. Guo, Y. Chen, D. Wu, R. Zhao, J. Tang, Z. Ma, C. Xue, W. Zhang, and J. Liu, "Plasmon-enhanced sensitivity of spin-based sensors based on a diamond ensemble of nitrogen vacancy color centers," *Opt. Lett.*, vol. 42, no. 3, pp. 403–406, 2017.

[10] H. Guo, Q. Zhu, J. Tang, F. Nian, W. Liu, R. Zhao, F. Du, B. Yang, and J. Liu, "A temperature and humidity synchronization detection method based on microwave coupled-resonator," *Sens. Actuators B, Chem.*, vol. 261, pp. 434–440, May 2018.

[11] X. Li and Q. Xu, "A reliable fusion positioning strategy for land vehicles in GPS-denied environments based on low-cost sensors," *IEEE Trans. Ind. Electron.*, vol. 64, no. 4, pp. 3205–3215, Apr. 2017.

[12] Z. Chen, W. Chen, X. Liu, and C. Song, "Fault-tolerant optical flow sensor/SINS integrated navigation scheme for MAV in a GPS-denied environment," *J. Sensors*, Sep. 2018, Art. no. 9678505. doi: 10.1155/2018/9678505.

[13] C. Shen, Z. Bai, H. Cao, K. Xu, C. Wang, H. Zhang, D. Wang, J. Tang, and J. Liu, "Optical flow sensor/INS/magnetometer integrated navigation system for MAV in GPS-denied environment," *J. Sensors*, Jan. 2016, Art. no. 6105803. doi: 10.1155/2016/6105803.

[14] L. Zhang, Z. Xiong, J. Lai, and J. Liu, "Optical flow-aided navigation for UAV: A novel information fusion of integrated MEMS navigation system," *Optik*, vol. 127, no. 1, pp. 447–451, 2016.

[15] P. Agrawal, A. Ratnoo, and D. Ghose, "Inverse optical flow based guidance for UAV navigation through urban canyons," *Aerosp. Sci. Technol.*, vol. 68, nos. 163–178, Sep. 2017.
[16] L. R. G. Carrillo, I. Fantoni, E. Rondon, and A. Dzul, "Three-dimensional position and velocity regulation of a quad-rotorcraft using optical flow," *IEEE Trans. Aerosp. Electron. Syst.*, vol. 51, no. 1, pp. 358–371, Jan. 2015.
[17] M. H. Tak and J. H. Young, "Localization and autonomous navigation using GPU-based sift and virtual force for mobile robots," *Trans. Korean Inst. Elect. Eng.*, vol. 65, no. 10, pp. 1738–1745, 2016.
[18] Q. Zhao, B. Zhang, S. Lyu, H. Zhang, D. Sun, G. Li, and W. Feng, "A CNN-SIFT hybrid pedestrian navigation method based on first-person vision," *Remote Sens.*, vol. 10, no. 8, p. 1229, 2018.
[19] Q. Zhu, C. Liu, and C. Cai, "A novel robot visual homing method based on SIFT features," *Sensors*, vol. 15, no. 10, pp. 26063–26084, 2015.
[20] Y. Yang, X. Hu, L. Xu, and F. Wang, "SIFT saliency analysis for matching repetitive structures," *Math. Problems Eng.*, Dec. 2017, Art. no. 2878930. doi: 10.1155/2017/2878930.
[21] T. Crivelli, M. Fradet, P.-H. Conze, P. Robert, and P. Pérez, "Robust optical flow integration," *IEEE Trans. Image Process.*, vol. 24, no. 1, pp. 484–498, Jan. 2015.
[22] Y. Niu, Z. Xu, and X. Che, "Dynamically removing false features in pyramidal Lucas-Kanade registration," *IEEE Trans. Image Process.*, vol. 23, no. 8, pp. 3535–3544, Aug. 2014.
[23] X. Guo, J. Tang, J. Li, C. Wang, C. Shen, and J. Liu, "Determine turntable coordinate system considering its non-orthogonality," *Rev. Sci. Instrum.*, vol. 90, no. 3, 2019, Art. no. 033704.
[24] Z. Wang, J. Zhou, J. Wang, W. Du, J. Wang, X. Han, and G. He, "A novel fault diagnosis method of gearbox based on maximum kurtosis spectral entropy deconvolution," *IEEE Access*, vol. 7, pp. 29520–29532, 2019.
[25] Z. Wang, W. Du, J. Wang, J. Zhou, X. Han, Z. Zhang, and L. Huang, "Research and application of improved adaptive MOMEDA fault diagnosis method," *Measurement*, vol. 140, pp. 63–75, Jul. 2019.
[26] M. Qasaimeh, H. Saleh, B. Mohammad, T. Tekeste, and M. Ismail, "A novel SIFT architecture and ASIC implementation for real time SOC application," *Analog Integr. Circuits Signal Process.*, vol. 99, no. 2, pp. 325–338, 2019.
[27] X. Guo, J. Tang, J. Li, C. Shen, and J. Liu, "Attitude measurement based on imaging ray tracking model and orthographic projection with iteration algorithm," *ISA Trans.*, to be published. doi: 10.1016/j.isatra.2019.05.009.
[28] Z. Wang, G. He, W. Du, J. Zhou, X. Han, J. Wang, H. He, X. Guo, J. Wang, and Y. Kou, "Application of parameter optimized variational mode decomposition method in fault diagnosis of gearbox," *IEEE Access*, vol. 7, pp. 44871–44882, 2019.
[29] Y. Zhang, C. Shen, J. Tang, and J. Liu, "Hybrid algorithm based on MDF-CKF and RF for GPS/INS system during GPS outages," *IEEE ACCESS*, vol. 6, pp. 35343–35354, 2018.
[30] Z. Zhang, "Camera calibration with one-dimensional objects," *IEEE Trans. Pattern Anal. Mach. Intell.*, vol. 26, no. 7, pp. 892-899, Jul. 2004.

XIAOCHEN LIU was born in Wuqing, Tianjin, in 1995. He received the B.S. degree from the School of Instrument and Electronics, North University of China. He is currently pursuing the M.S. degree at the College. His research direction is visual navigation and related signal processing.

XIAOTING GUO received the Ph.D. degree from the School of Precision Instrument and Opto-Electronics Engineering, Tianjin University, China, in 2018. She is currently a Lecturer with the School of Instrument and Electronics, North University of China. Her research interests include navigation systems and related signal processing.

DONGHUA ZHAO is currently pursuing the Ph.D. degree with the College. She is also a Lecture with the School of Instrument and Electronics, North University of China. Her research direction is bio-inspired navigation.

HUILIANG CAO received the Ph.D. degree in instrument science and technology from Southeast University, Nanjing, China, in 2014, and the Ph.D. degree from the Georgia Institute of Technology, Atlanta, GA, USA, in 2012. He is currently an Associate Professor with the North University of China, Taiyuan, China. His current research interest includes the areas of MEMS inertial devices.

JUN TANG received the Ph.D. degree from the Department of Physics, National Technical University of Athens, in 2010. He is currently a Professor with the School of Instrument and Electronics, North University of China. His research interests include MOEMS gyroscope and polarization navigation.

CHENGUANG WANG received the Ph.D. degree from the North University of China, Shanxi, China, in 2015. He is currently an Associate Professor with the School of Information and Communication Engineering, North University of China. His research interests include polarization navigation and related signal processing.

CHONG SHEN received the Ph.D. degree from the School of Instrumentation Science and Engineering, Southeast University, China, in 2014. He is currently an Associate Professor with the School of Instrument and Electronics, North University of China. His research interests include navigation systems and related signal processing.

JUN LIU received the Ph.D. degree from the Beijing Institute of Technology, Beijing, China, in 2001. He was a Postdoctoral Researcher with Peking University, from 2003 to 2007. His research interests focus on MOEMS and Micro/Nano Sensor. As the Team Leader, he has worked around 20 different projects funded by the National "863" Project, National Nature Funds, and National 973 Project et al. He is also a technical committee member in several international conferences in the above fields. He has authored or coauthored more than 160 publications in international journals.